Fluid inclusion and isotopic constraints on the genesis of vein-quartz gold deposits of the Ipitinga Auriferous District, SE-Guyana Shield, Brazil

Evandro L. Klein[1], Jean-Michel Lafon[2], Chris Harris[3], Reinaldo S.C. Brito[4], Paulo Vasconcelos[5]

(1) CPRM - Serviço Geológico do Brasil, Av. Dr. Freitas, 3546, CEP 66095-110, Belém - PA, Brasil.
e-mail: eklein@be.cprm.gov.br
(2) Laboratório Para-Iso, Universidade Federal do Pará, Belém - PA, Brasil
(3) University of Cape Town, South Africa
(4) CPRM - Serviço Geológico do Brasil, Brasília - DF, Brasil
(5) University of Queensland, Brisbane, Australia

Abstract

The Ipitinga Auriferous District (SE-Guyana Shield, NW-Pará state) contains vein-quartz gold occurrences hosted in Paleoproterozoic metavolcano-sedimentary sequences and associated granitoids, especially near the contact between the granitoids and the supracrustal rocks. The structurally-controlled deposits are hosted in ductile shear zones and in foliation planes of the host rocks, have sericitization as the main important proximal alteration, and have small amounts of sulfide minerals in the ore paragenesis. Fluid inclusion types and properties are similar in most of the deposits. The aqueous-carbonic inclusions, with small to moderate amounts of CH_4 (locally C_2H_6) are the predominant types. These inclusions have low salinity (~5 wt. % NaCl equiv.) and homogenized between 290° and 355°C. Carará differs from this pattern in that it shows only water-free CO_2-bearing inclusions, the origin of which is still uncertain. Oxygen and hydrogen isotope compositions overlap the fields of magmatic and metamorphic waters, except at Carará that clearly shows a metamorphic source for the hydrothermal fluid. Integrated geologic characteristics, and fluid inclusion and isotopic results are consistent with the class of orogenic gold deposits. The characteristics reported in the literature for the Serra do Ipitinga Au occurrence strongly differs from those presented by the studied deposits in the district and probably belong to another class of deposit. Pb-Pb and ^{40}Ar-^{39}Ar systematics have not succeed in determining the age of the mineralizing event in the Ipitinga Auriferous District, but bracketed a time window for mineralization between 1940 and 2030 Ma.

Keywords: gold, fluid Inclusions, stable Isotopes, Pb isotopes, Ar-Ar, Amazonian Craton.

Resumo

O Distrito Aurífero de Ipitinga, no sudeste do Escudo das Guianas (noroeste do estado do Pará), contém ocorrências de ouro associadas a veios de quartzo hospedados em rochas vulcanossedimentares paleoproterozoicas e em granitóides a elas associados, especialmente quando próximo ao contato com rochas supracrustais. Os depósitos apresentam similaridades em termos de estruturas hospedeiras, que são principalmente zonas de cisalhamento dúctil e a foliação das rochas encaixantes, presença de sericita como alteração proximal mais importante e pequena quantidade de sulfetos na paragênese. As inclusões fluidas apresentam características relativamente similares entre os depósitos, predominando os tipos aquo-carbônicos com pequena contribuição de outros voláteis na fase gasosa (traços a quantidades moderadas de CH_4 e, localmente, traços de C_2H_6). Esses fluidos têm baixa salinidade (~5 % NaCl. equiv.) e homogeneizaram entre 290° e 355°C. O depósito de Carará difere em termos de fluidos, contendo apenas inclusões de CO_2 ($\pm N_2$), sem H_2O, cuja origem é ainda incerta. Isótopos de oxigênio e hidrogênio indicam superposição de fontes magmática e metamórfica, com exceção de Carará, cuja fonte é claramente metamórfica. O conjunto de dados geológicos e os resultados de inclusões fluidas e isótopos estáveis são consistentes com a classe de depósitos orogênicos de ouro. A ocorrência de Serra do Ipitinga, descrita na literatura, difere desse padrão e provavelmente pertence a outra classe de depósito. Sistemas radiogênicos (Pb-Pb, ^{40}Ar-^{39}Ar) não definiram a idade da mineralização, mas permitem o estabelecimento de limites para a mesma, entre 1940 e 2030 Ma.

Palavras-chave: ouro, inclusões fluidas, isótopos estáveis, isótopos de Pb, Ar-Ar, Cráton Amazônico.

INTRODUCTION

The Ipitinga Auriferous District is located in NW-Pará State (Brazil), SE-Guyana Shield (Fig. 1). The district contains a few known vein quartz-gold occurrences and deposits (Divisão, Nova Esperança, igarapé do Inferno, Mamão, Castanhal, Limão, Catarino, and Carará). Klein & Rosa-Costa (2003) described geologic aspects of these deposits, such as host rock (predominantly metavolcano-sedimentary, with associated granitoids), host structure (a ductile shear zone that separates tectonic domains), vein texture and proximal hydrothermal alteration, in addition to vein style, formation and deformation. Those authors observed many similarities between the deposits and concluded that they belong to a single class of deposits and that their geologic characteristics are compatible with the class of orogenic gold (e.g., Groves *et al*. 2003). In the same region, Faraco *et al*. (2006) presented a fluid inclusion study in a vein quartz occurrence at Serra do Ipitinga and also interpreted the mineralization as belonging to the class of orogenic gold, spatially associated with a precursor volcanogenic sulfide Cu-Au mineralization.

In this paper we present fluid inclusion, oxygen, hydrogen, carbon, and lead isotopes compositions and ^{40}Ar-^{39}Ar data for some of these vein quartz-gold deposits. Despite the reconnaissance character of the study, the results help in the understanding of genetic aspects of gold mineralization in the Ipitinga Auriferous District, such as the physico-chemical (P-T-composition) conditions of ore formation and potential sources for fluids and solutes.

GEOLOGIC SETTING

The Ipitinga Auriferous District is located in the Paleoproterozoic Maroni-Itacaiunas orogenic belt. A few tectonic domains have been defined within this belt, and the auriferous district is located more precisely within the Carecuru domain, close to the limit of this terrane with the Jari domain (Rosa-Costa *et al*. 2003, 2006). The Carecuru domain is described as being a Paleoproterozoic granitoid-greenstone terrane that surrounds an Archean granulitic nucleus of 2597±4Ma (Rosa-Costa *et al*. 2003).

The Carecuru domain (Fig. 1) is composed predominantly of calc-alkaline diorites and tonalites of the Paru-Maratiá Complex and Carecuru Intrusive Suite of 2150±1 Ma and 2140±1Ma, respectively (Rosa-Costa *et al*. 2003), and of more or less continuous belts of supracrustal rocks. These belts comprise the mafic-ultramafic metavolcanic schists, metasedimentary schists, iron formations, and quartzites of the Ipitinga Group of 2265±34 Ma (Sm-Nd isochrone age, McReath & Faraco 2006), and mafic to intermediate metavolcanic rocks of the Fazendinha, Treze de Maio and Cuiapocu sequences. The granitoids show variable deformation, from preserved igneous textures to a pervasive foliation, whereas the supracrustal sequences underwent greenschist to amphibolite facies metamorphic conditions (Rosa-Costa *et al*. 2003, McReath & Faraco 2006).

The association of voluminous calc-alkaline granitoids with intermediate to basic metavolcanic rocks, the proximity of the Carecuru domain of the Archean Jari domain, and the Nd isotope evidence suggesting involvement of Archean crust in the genesis of the Paleoproterozoic granitoids led Rosa-Costa *et al*. (2006) to interpret the Carecuru domain as a continental magmatic arc. Other orogenic granitoid plutons of variable compositions intruded in both Jari and Carecuru domains by 2146±3Ma (Rosa-Costa *et al*. 2003).

The NW-SE-trending Ipitinga shear zone represents the boundary zone between the Carecuru and Jari domains (Fig. 1). This zone is a wide structural system made up of major and subsidiary faults and ductile shear zones (first and second order structures) that affected especially the supracrustal sequences, which are parallel to the strike of this fault/shear system, and has spatial relationship with the gold mineralization of the Ipitinga Auriferous District. This system has a complex history, involving early thrusting and late strike-slip displacement (Klein & Rosa-Costa 2003).

The regional foliation is parallel to the major tectonic discontinuities. However, in places, it is parallel to the contacts between the supracrustal sequences and the granitoid plutons. This schistosity has overprinted primary structures of the rocks. A down dip to slightly oblique elon gation lineation is contained in the foliation planes, and slickenlines are also present, especially at the contact between veins and their host rocks. The strike-slip movement is evident along the limit between the Carecuru and Jari domains, overprinting early thrust structures and showing both dextral and sinistral kinematic features. However, in the inner portions of the Carecuru domain the supracrustal sequences show steep lineations, suggesting limited strike-slip influence during the ductile deformation. According to Klein & Rosa-Costa (2003), these structural elements record a compressive deformation event, with an early NE-SW shortening (D1) followed by the transcurrent deformation (D2).

ANALYTICAL PROCEDURES

The fluid inclusion study was carried out on doubly-polished samples of vein quartz. After petrographic examination, the microthermometric work was performed using a Chaixmeca heating-freezing stage at the Universidade Federal do Pará, in Belém, Brazil. Calibration was done with synthetic CO_2 and H_2O standards. Precision was estimated to be ± 0.3°C for runs below 40°C and ± 3°C for runs above 40ºC. Raman analyses were carried out at the Universidade Federal de Minas Gerais (UFMG),

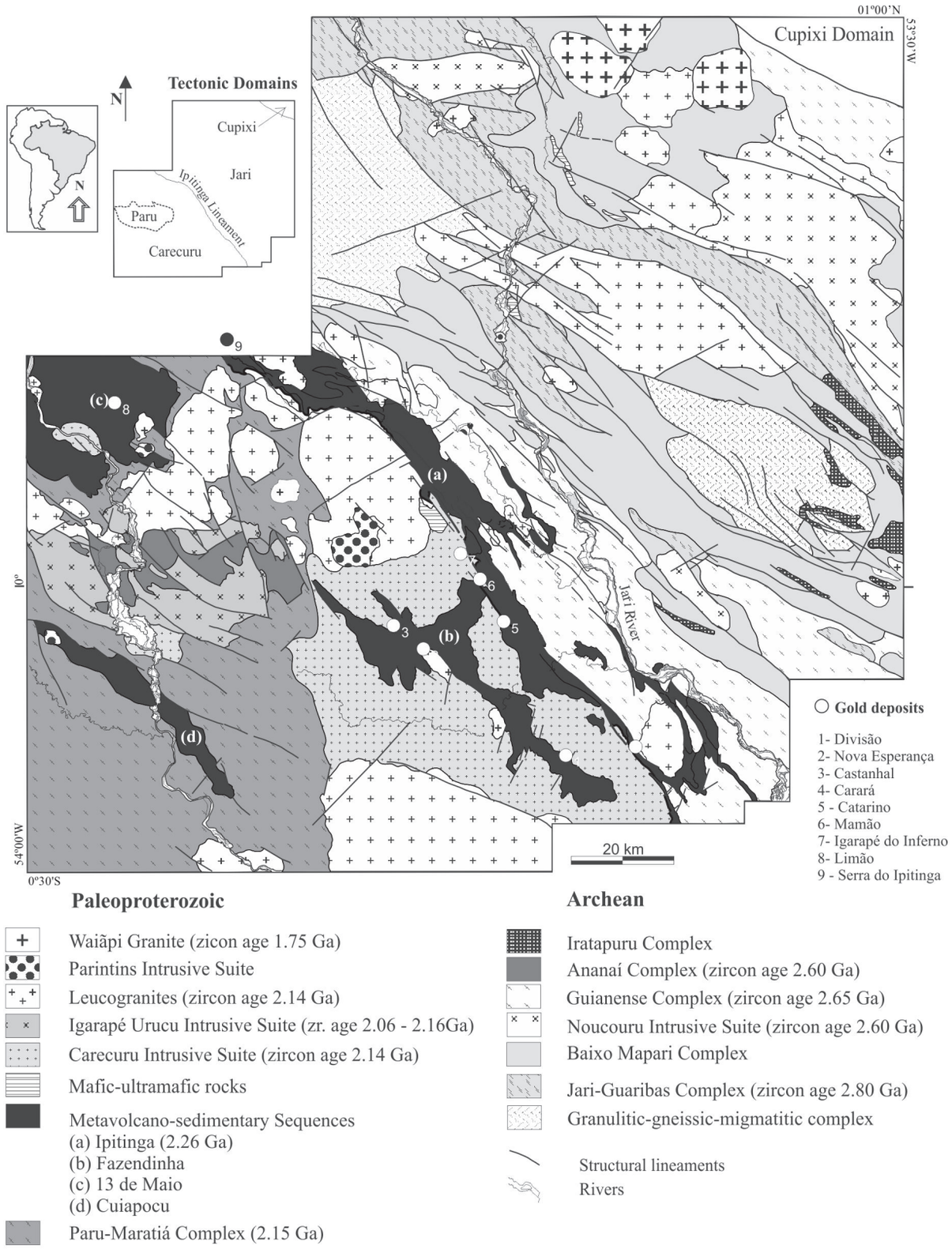

Figure 1. *Location map and geologic map of part of the SE-Guyana shield (modified from Rosa-Costa et al. 2006) and location of the gold deposits of the Ipitinga Auriferous District.*
Figura 1. *Mapa de localização e mapa geológico de parte da porção sudeste do Escudo das Guianas (modificado de Rosa-Costa et al. 2006) e localização dos depósitos auríferos do Distrito Aurífero de Ipitinga.*

in Belo Horizonte, Brazil, using a Dilor XY spectrometer equipped with multiple collectors. The excitation source was an Argon laser Ivanova 70-3 with a wavelength of 514.53µm and 150 mW of power. Integration time was 10 seconds, with ten accumulations for each spectral line. Calibration was done with mercury light.

Carbon, oxygen, and hydrogen isotope analyses were carried out at the Laboratoire des Isotopes Stables of the Université Jean Monnet (UJM), in Saint Etienne, France. Isotope ratios were measured using a Micromass-Isoprime gas-source mass spectrometer in dual-inlet mode. For oxygen isotope analysis of silicate minerals, two methods were employed, both using BrF_5 as reagent. The conventional fluorination method (Clayton & Mayeda 1963) was employed for hydrated minerals, and a CO_2 laser fluorination system (Harris *et al*. 2000) was used for quartz analysis. In both methods oxygen was converted to CO_2 by reaction with graphite. In the conventional method, samples were loaded into Ni-reaction vessels and degassed at 250°C for about 2 hours. Oxygen was produced by reacting 5-10 mg of samples with BrF_5 at 550°C for 8-12 hours. An internal standard (MQ quartz, $\delta^{18}O$ = +10.1‰) was analyzed to calibrate the data to the V-SMOW scale. The mean values obtained from repeated analyses MQ gave a difference of 0.3 per mil from the accepted value. In the laser system oxygen was produced by heating quartz grains weighing typically 2-4mg with a 40 W CO_2 laser in atmosphere of BrF_5. An internal standard (MONGT, $\delta^{18}O$ = +5.55‰) was analyzed to calibrate the data to the V-SMOW scale, and duplicates gave agreement within 0.2 per mil. Hydrogen was produced by heating 10-30mg of mineral concentrates in vacuum, following procedures described in Vennemann & O'Neil (1993) and using a CuO furnace. Water was purified cryogenically and then reduced to H_2 by reaction with "Indiana Zinc" at 450°C, according to procedures adapted from Coleman *et al*. (1982). An internal silicate standard (AM muscovite, δD = –30‰) gave a mean value of –30.5 per mil that was used to calibrate the data to the V-SMOW scale. Reproducibility is estimated to have been better than 4 per mil. Inclusion fluids (H_2O, CO_2) were liberated by decrepitation of fluid inclusions during heating of 1-2 g of quartz (fragments <3 mm) at temperatures >800°C. The quartz fragments were previously cleaned with HCl and HNO_3 and degassed at 200° and 300°C. The obtained water and CO_2 were trapped cryogenically and analyzed for hydrogen and carbon isotopes, respectively. The $^{13}C/^{12}C$, $^{18}O/^{16}O$, and D/H ratios are reported in the delta notation, normalized to the PDB (carbon) and V-SMOW (oxygen and hydrogen) scales.

Pb isotope analyses were carried out at the Laboratório de Geologia Isotópica – ParaIso – of the Universidade Federal do Pará, in Belém, Brazil. The experimental procedure used 20-70mg of sulfide minerals. The mineral concentrates were washed with distilled water and HCl and sample dilution was obtained by using a combination of HCl, HNO_3 and HBr (Rodrigues *et al*. 1993). The lead separation was done in Teflon columns containing DOWEX AG 1x8 (200-400mesh) resin through sequential adding of HBr and HCl. Pb was deposited in Re filaments with a combination of HCl + H_3PO_4 and the isotope composition obtained with VG ISOMASS 54E (pyrite samples) and Finnigan MAT262 (galena sample) mass spectrometers. For model ages calculation the Isoplot software (Ludwig 2003) was employed.

Ar-Ar analyses were performed at the UQ-AGES Laboratory of the University of Queensland, in Brisbane, Australia. The crushed material was cleaned in an ultrasonic bath for at least one hour and one half hour respectively with distilled water and ethanol in succession and then dried. Twenty to fifty grains 0.5 to 2 mm in size were hand-picked from the cleaned material using a binocular microscope. Five to 10 grains from each sample were placed into aluminum irradiation disks along with Fish Canyon sanidine standards (28.02±0.28Ma; Renne *et al*. 1998). The irradiation disks were closed with aluminum covers, wrapped in aluminum foil and vacuum heat sealed into quartz vials. The quartz vials were irradiated for 14 hours at the B-1 CLICIT facility at the Radiation Center, Oregon State University, U.S.A. After a decay period, one to three grains from each sample were analyzed by laser incremental $^{40}Ar/^{39}Ar$ step heating following procedures detailed in Vasconcelos *et al*. (2002).

SUMMARY OF THE DEPOSITS GEOLOGY

This section summarizes the main characteristics of the gold deposits, as described by Klein & Rosa-Costa (2003). Accordingly, the gold-quartz veins are hosted by Paleoproterozoic metavolcano-sedimentary sequences and coeval granitoids. Hosting structures are mainly the regional foliation and moderate to high-angle reverse-oblique shear zones and faults, spatially related to major, terrane-boundary shear zones. Most of the granitoid-hosted deposits occur close to the contact of the granitoids with the supracrustal rocks (Fig. 1). The main structural styles are shear/fault-fill veins, and subordinately extensional-oblique veins. Sericitization is the dominant silicate alteration, whereas pyrite is the main sulfide mineral. The veins are syn- to late tectonic and emplaced at moderate depths, after the metamorphic peak, while the hosting structures were still active, during regional episode of progressive compressional deformation. Variation in orientation, intensity of deformation and vein style were attributed to temporal relationships between veins and hosting structures, processes occurring after vein formation, intrusion of granitoids in the supracrustal sequences, and regional and local field stress (Klein & Rosa-Costa 2003).

Divisão - The studied vein is up to 1 meter thick, vertical and strikes to N5ºE. It is composed of milky massive quartz and contains minor amounts of chalcopyrite, pyrite and galena. The vein is associated with an ore zone striking N85ºW and dipping 40ºNE that varies in style from a single, up to 1 meter-thick vein, to an anastomosed set of thin and discontinuous veinlets and enclosing altered host rock. They are strongly fractured, probably due to late cataclasis, and internally show medium-grained (2-3mm) quartz. The hosting shear zone cuts undeformed biotite-rich tonalite of the Carecuru Intrusive Suite close to its contact with mafic metavolcanic rocks and amphibolites.

Nova Esperança - Gold mineralization is associated with a 50cm-thick quartz vein that strikes N85ºW and dips 10ºSW. The vein is hosted by a brittle structure that cut across an undeformed, coarse-grained monzogranite belonging to an undivided unit of orogenic granitoids. The vein shows laminated to saccharoidal texture and minor concentrations of pyrite. In places, it consists of coarse-grained, milky and massive quartz, which lacks sulfide minerals. The laminated texture consists of quartz laminae separated by thin discontinuity surfaces defined by aggregates of comminuted quartz. Internally, the laminae show saccharoidal and massive textures. Sericite occurs in fractures of the quartz.

Igarapé do Inferno - Mineralization is associated with a sulfide-bearing, 50cm-thick coarse-grained, saccharoidal quartz vein that strikes N50ºW and dips 58ºSW. Fine-grained subhedral pyrite grains occur as disseminations along the vein. The host rock is an undeformed monzogranite (similarly to Nova Esperança) that belongs to an undivided unit of orogenic granitoids close to its contact with mafic-ultramafic rocks of the Ipitinga Group. This host rock shows a relatively symmetrical hydrothermal envelope up to 3m-thick around the vein with relics of sericite. Hydrothermal sericite also fills fractures in the vein as well. The vein is discontinuous and occasionally only the hydrothermally altered granitoid is observed.

Mamão - The Mamão deposit is composed of a series of veins hosted in a pelitic metasedimentary rock of the Ipitinga Group. The veins align along a NW-SE-trending structure that can be traced for ~400m, and parallels the regional foliation. This foliation strikes N30º-45ºW and dips to 60ºSW, with local inflections with variable dips to north and northeast, suggesting that the foliation is folded. Locally, altered amphibole- and serpentine-bearing schists are present. Gold occurs in massive to saccharoidal quartz veins and disseminated in the enclosing hydrothermal halos. These halos are up to 4 m wide and are composed of sericite and quartz. Commonly, tiny fractures that cut both the quartz vein and the altered wall-rock are filled with sericite. The veins are either subparallel to, or cut across the foliation.

Castanhal - Mineralization is associated with two quartz veins hosted by a highly strained pelitic metasedimentary rock of the Fazendinha Sequence. One quartz vein is up to 20cm-thick with an attitude of N50º-60ºE/80ºSE, which is subparallel to the strike of the foliation of the host rock. The vein is surrounded by a centimeter-wide hydrothermal envelope composed of inner sericitic and outer chloritic alteration. This vein shows a laminated texture, defined by the alternation of quartz laminae separated by discontinuity surfaces that are parallel to the vein strike. There is no clear microscopic difference between adjacent laminae, and no evidence of dislocation along the surfaces could be characterized.

A second massive and fractured vein strikes N30ºW and dips 60ºSW, cutting across the foliation of the host rock, which strikes E-W, dipping 85ºS, suggesting that foliation is folded. The vein is 40cm-thick and is surrounded by an alteration halo of sericite a few decimeters wide. Irregularly-shaped pockets of hydrothermally altered host rock locally occur in the proximity of the vein.

No crosscutting relationships could be observed between the two veins. Klein & Rosa-Costa (2003) suggested that they can be interpreted either as a single vein that has been transposed and disrupted during progressive stages of strain within a strike-slip shear zone, or as a set of shear and extensional-oblique veins, respectively. The foliation of the host rock is discordant with respect to the regional structural grain, which may be attributed to the emplacement of granitoids of the Carecuru Intrusive Suite (Fig. 1).

Limão - This prospect occurs in the northwestern portion of the district (Fig. 1), close to the Au showing described in Faraco *et al*. (2006). At Limão gold mineralization occurs within a vein that ranges from 0.5 to 2 m in thickness, with a minimum length of 50 m. The vein is fringed by a few cm-thick sericitic hydrothermal halo, which highlights the limits of the host ductile shear zone. Medium-grained pyrite occurs along the vein-wall rock contact, and very fine-grained pyrite is disseminated in the vein. Gold seems to be restricted to the vein and to its contact with the host banded iron-formation that belongs to the Treze de Maio Sequence.

The vein strikes N80ºW, and dips 75º to SW, being parallel to the shear zone. Within the vein, the quartz grains are elongated down to the foliation dip and striations in the vein walls indicate reverse movement, characterizing the host structure as a high-angle reverse shear zone. The internal structure of the vein varies across the strike. At the hanging wall the vein shows a laminated/schistose aspect, with ribbon quartz alternating with slivers of altered wall-rock. In the intermediate positions between the hanging wall and the center, the vein is laminated but not schistose, with individual quartz laminae separated by discrete slip surfaces. In the core, the vein is massive, becoming laminated again towards the footwall.

Catarino - The Catarino occurrence is characterized by a shallow dipping (up to 35ºSW) ore zone composed of subparallel quartz-veinlets, ranging from 3 to 10cm in thickness. The host rock is a muscovite-bearing quartzite similar to that found at Carará (see below), which strikes to N20ºW. The milky quartz shows massive, saccharoidal and locally laminated textures. Wall-rock alteration is characterized by coarse-grained muscovite

in addition to tourmaline and quartz. Tourmaline occurs either at the contact between vein and wall rock or separating laminae of quartz. Free gold is occasionally visible, occurring as platy, irregularly-shaped to rather rectangular particles, up to 0.5mm long (rarely achieving 2.5mm).

A variation in the intensity of strain between the host rock and the ore zone was not recognized. Therefore, the vein sets were interpreted to have formed by dilation of the foliation (Klein & Rosa-Costa 2003).

Carará - The Carará deposit holds reserves of 10 t of gold averaging 21.2 g/ton (Carvalho et al. 1991). The mineralized quartz vein is hosted by a strained tourmaline- and muscovite-bearing quartzite of the Ipitinga Group (Fé em Deus Formation). The quartzite shows a steeply-dipping (75º-85º) foliation that strikes to NNW-SSE and down the dip to slightly oblique (70º/S30ºW) stretching lineations. Gold mineralization at Carará is restricted to a 460m-long, 0.15 to 3m-thick quartz vein emplaced in the central portion of the hosting shear zone, and is subparallel to the regional foliation. This vein contains variable gold grades and the terms high-grade quartz (HGQ) and low-grade quartz (LGQ) are used here to describe these variation. The vein is surrounded by a 10-50 cm-thick hydrothermal halo with microfractures filled with muscovite and tourmaline, which is called tourmaline-rich vein (TRV). Vein quartz shows massive to saccharoidal textures and tourmaline is better developed at the contact between the vein and the wall rock. Muscovite and tourmaline grains show an elongation lineation that indicates reverse to reverse-oblique dislocation along the vein. These structural elements are consistent with a high-angle reverse shear zone, and indicate that the shear zone was active at the time of vein formation.

FLUID INCLUSIONS

The fluid inclusion study was concentrated in samples from Divisão (116 fluid inclusions), Nova Esperança (129 fluid inclusions) and Mamão (146 fluid inclusions). Vein samples from Castanhal, igarapé do Inferno, Catarino and Limão were also examined but these have shown to be strongly deformed, with almost all fluid inclusions being eliminated during the recrystallization of quartz. Data from Carará and Serra do Ipitinga have been compiled from the literature.

Based on the bulk composition, number of phases, and behavior in room and sub-zero temperatures, three types of fluid inclusions have been identified in the investigated deposits. Type 1 comprises one-phase, dark carbonic inclusions. Type 2 are two-phase H_2O-CO_2-bearing inclusions (aqueous-carbonic). Type 3 are two-phase H_2O-salts inclusions (aqueous).

Microthermometry involved measurements of CO_2 melting temperature ($TmCO_2$), clathrate melting temperature (Tmclat), CO_2 homogenization temperature ($ThCO_2$), temperature of first observed melting (~eutectic) (Te), ice melting temperature (Tmice), total homogenization temperature (Th L or V, where L stands for liquid, and V for vapor). In addition, VCO_2 is the volumetric proportion of the carbonic phase (vol. CO_2/vol. total, in percentage), and Vg is the vapor volume (vol. H_2O vapor/vol. total, in percentage) in aqueous inclusions. Fluid compositions and isochores were calculated with the aid of the FLINCOR computer program (Brown 1989).

Divisão - Quartz at Divisão is porphyroclastic, irregularly shaped and shows moderate to strong undulose extinction and some deformation lamellae. Subgrains occupy the interstices between the porphyroclasts and form 50% of the vein volume. The fluid inclusions show random distribution or form wide tri-dimensional sets of two-phase inclusions and trails of one-phase inclusions. In places, inclusions show evidence of necking-down. Inclusion sizes vary mostly between 5 and 12 µm, and the predominant shapes are ellipsoidal, polygonized, and irregular.

Type 1 is abundant and prevails over Type 2. Type 2 shows VCO2 between 20 and 90% (with peaks at 30 and 70%). Types 1 and 2 occur in close association in a single cluster or trail and represent a single fluid inclusion assemblage (FIA).

The CO2 melting temperature in types 1 and 2 occurred between -57.1° and -66.4°C with the same distribution in the two types and with a sharp modal value of -57.8°C (Fig. 2A). These TmCO2 values indicate the presence of other components in the carbonic phase in addition to CO_2, which has been confirmed by the micro-Raman analyses that detected 3-24% of CH4 in the volatile phase (Table 1). The partial homogenization of the carbonic phase occurred between -37.7° and +23.2°C, with most of values being higher than -3.4°. Although both types show negative values as low as -37°C, most of Type 2 inclusions have $ThCO_2$ greater than 8°C (Fig. 2B).

In Type 2 inclusions, the clathrates melted in the range of 5.9° to 9.8°C and show a sharp mode at 6.6°C (Fig. 2C), corresponding to a salinity of 6.1 wt. % NaCl equiv. Despite the presence of CH_4, which might cause the underestimation of salinity (Collins 1979), the low molar proportion of CH_4 allows us to assume that the estimated values are a good approximation of the salinity of the fluid. The final homogenization of Type 2 inclusions occurred in a wide range, from 278° to 413°C both to liquid and vapor. The frequency distribution of Th shows two major peaks at 295° and 355°C, and a minor one at 415°C (Fig. 2D).

Type 3 aqueous inclusions show Vg of 5-10% and only rarely occur in a same microscopic domain with types 1 and 2, representing a distinct assemblage. These inclusions have ice melting temperatures ranging from -0.3° to -5.2°C (Fig. 2E), implying salinities between 0.5 and 8.1 wt. % NaCl equiv., and no eutectic melting has been observed. The final homogenization occurred at a wide range of temperature, between 74° and 253°C range (Fig. 2F), always to the liquid.

Table 1. *Composition of the volatile phase of fluid inclusions from gold-quartz vein deposits of the Ipitinga Auriferous District based on Raman analyses.*

Tabela 1. *Composição da fase volátil de inclusões fluidas em depósitos auríferos em veios de quartzo do Distrito Aurífero de Ipitinga.*

Deposit	sample	FI	type	CO2	CH4	N2	C2H6
Divisão	78B	3/2	1	97	3	nd	nd
		3/3	1	76	24	nd	nd
Nova Esperança	85B	1/1	2	98	2	nd	nd
Mamão	81A	2/1	2	~100	nd	nd	tr
		2/2	2	~100	tr	nd	nd
Carará	80A	3/1	1	~100	tr	nd	tr
		3/2	1	~100	tr	nd	tr
		3/3	1	~100	nd	nd	tr
		3/4	1	~100	nd	nd	tr
		3A/6	1	98	nd	2	nd
		3A/7	1	100	nd	nd	nd
	80B2	1	2	nd	nd	~100	nd

FI. fluid inclusion; nd – not detected; tr - trace

DISCUSSION

The microthermometric results confirmed the petrographic evidence that types 1 and 2 form a single fluid inclusion assemblage. The CO_2- and CH_4-bearing inclusions show a positive correlation between $ThCO_2$ and $TmCO_2$ (Fig. 3A). Two mechanisms may explain this behavior (e.g., Klein *et al*. 2000): (1) oxidation of an early fluid at low oxidation-state, following the reaction $CH_4 + 2O_2 = CO_2 + H_2O$; or (2) reduction of an initially more oxidized fluid exemplified by the hydration reaction $CO_2 + 4H_2 = CH_4 + 2H_2O$. The predominance of inclusions with high $ThCO_2$ and $TmCO_2$ strongly indicates that the first mechanism has occurred.

The large variation in $ThCO_2$ implies very variable CO_2 densities, from 1.108 to 0.737g/cm^3. In individual trails or clusters, however, these variations are lower than 6°C. This also supports the interpretation of an evolving fluid with decreasing CH_4/CO_2 ratio. The oxidation might be related to phase separation. During phase separation (fluid immiscibility) of a CO_2-CH_4-H_2O-salt fluid, the CH_4 content of the fluid decreases toward the end of the process in response to the higher gas distribution coefficient of the CH_4 in relation to CO_2 (Drummond & Ohmoto 1985).

The two major, and one minor, peaks of Th (Fig. 2D), combined with absence of Tmclat variation (Fig. 2C), may represent cooling of the fluid with two main phases of trapping. This also precludes mixing. However, this multimodal distribution may also represent post-trapping changes such as necking down (e.g., Touret 1991) or leakage, which is supported by the vertical trend presented in the Tmclat versus Th plot (Fig. 3B). Accordingly, fluid trapping occurred mainly at about 290°C in response to phase separation, whereas the other peaks represent necking down. Furthermore, assuming phase separation, the Th values represent the true trapping temperature of the fluid. At these conditions trapping pressures are estimated to be at about 2.0-2.5kbar (Bowers & Helgeson 1983).

Nova Esperança - The studied vein quartz exhibits laminated texture and the quartz grains are fragmented and show undulose extinction. Most of the fluid inclusions occur in clusters of randomly distributed inclusions, with sizes ranging from 6 to 35δm, chiefly from 12 to 15δm in size. Many inclusions show evidence of necking down.

The largely predominant inclusions are Type 2 two-phase H_2O-CO_2-bearing inclusions with VCO_2 mostly between 40-70%. Type 1, one-phase, dark carbonic nclusions are subordinate. Types 1 and 2 occur in close association in a same cluster and represent a single fluid inclusion assemblage. Type 3 inclusions are rare and have been described in a single domain of the host quartz. These inclusions show Vg <5%.

The microthermometric work showed that $TmCO_2$ in Types 1 and 2 inclusions occurred between -58.9° and -57.9°C with a modal value of -57.9°C (Fig. 4A). This indicates that CO_2 is the predominant volatile phase, with small proportions of an additional component. This phase has been determined to be CH_4 (2% of the volatile phase) by the micro-Raman analysis (Table 1). The partial homogenization of the carbonic phase occurred in the 4.7°-21.1°C range, always to liquid. The frequency of distribution of $ThCO_2$ is asymmetric and highly skewed to the left (Fig. 4B).

Clathrates in Type 2 fluid inclusions melted in a relatively wide range of temperatures, between 0.1° and 7.4°C (Fig. 4C), corresponding to salinities of about 15.4 to 4.6 wt.% NaCl equivalent. A peak, however, is observed at 6.5°C, which gives a principal salinity of 6.2 wt.% NaCl equivalent. The final homogenization of Type 2 inclusions occurred both to liquid and vapor between 248° and 419°C. Although not being clearly bimodal, most of the values fall around 290° and 320°C (Fig. 4D).

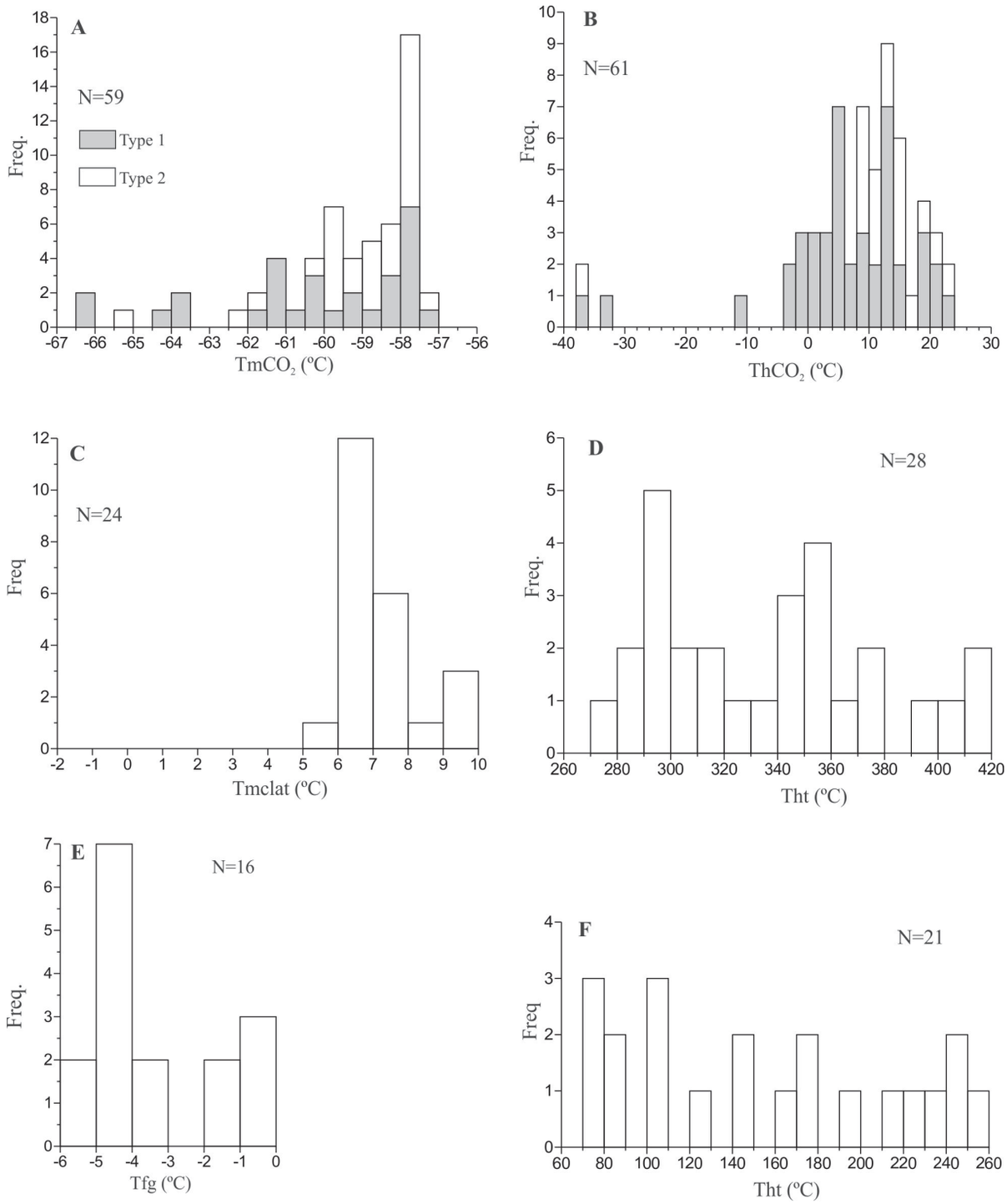

Figure 2. *Frequency histograms showing the distribution of microthermometric properties of fluid inclusions from Divisão.*
Figura 2. *Histogramas de frequência mostrando a distribuição das propriedades microtermométricas das inclusões fluidas em Divisão.*

Table 2. *Stable isotope data from vein minerals of gold deposits from the Ipitinga Auriferous District.*
Tabela 2. *Dados de isótopos estáveis em minerais de veios auríferos do Distrito Aurífero de Ipitinga.*

			silicates		fluid inclusions	
deposit	**sample**	**mineral**	$\delta^{18}O$ (‰)	δD (‰)	$\delta^{13}C_{CO2}$ (‰)	δD_{H2O} (‰)
Divisão	EK78B	quartz	+11.3			
Nova Esperança	EK85B	quartz	+12.9		-4.6	-76
	EK85C	quartz	+13.9		0.0	-43
Igarapé Inferno	LT178A	quartz	+13.9			
Mamão	EK81A	quartz	+12.6		-2.7	-49
	EK81B	quartz	+13.5		nd	-75
	EK81C	quartz	+12.9		nd	-58
	EK81D	quartz	+12.9		nd	-62
Castanhal	EK82A	quartz	+13.0		-30.2	-66
	EK82B	quartz	+12.6			
Limão	EK79B	quartz	+13.9			
	EK79C	quartz	+13.2		-25.5	-60
	EK79Ds	quartz	+13.1		-29.0	-51
	EK79Dw	quartz	+13.4			
Catarino	EK106	quartz	+12.3			
	EK106	tourmaline	+10.3			
	EK106	muscovite	+9.9	-38		
	EK106E	quartz	+11.0			
	EK106F	quartz	+11.2			
	EK106M1	muscovite	+10.6	-55		
	EK106M2	muscovite	+9.6	-53		
Carará	80A1	quartz	+11.8		-3.4	nd
	80A1	tourmaline	+10.1	-77		
	80A1	muscovite	+9.3	-40		
	80A2	quartz	+12.4			
	80C1	quartz	+12.0		-3.2	-33
	80C2	quartz	+12.7			
	80B1	quartz	+11.0		-14.6	-61
	80B1	tourmaline	+8.5	nd		
	80B2	quartz	+10.6			
	80B2	tourmaline	+9.3	-71		

The few Type 3 aqueous inclusions showed ice first melting temperature (~Teu) of -22.2° and -24.4°C, suggesting that the inclusions may belong to the H_2O-NaCl-KCl system (Hall *et al*. 1988). In these inclusions Tmice occurred between -0.5° and -5.9°C, implying salinities lower than 9.1wt. % of NaCl equiv., and the final homogenization below 170°C.

DISCUSSION

The small variation in $TmCO_2$ and the absence of correlation between $TmCO_2$ and $ThCO_2$ (Fig. 5A) indicate that a single fluid has been trapped. The absence of correlation in the Th versus Tmclat diagram (Fig. 5B) also precludes mixing. Despite the large range in $ThCO_2$, variations of this parameter within single clusters or trails

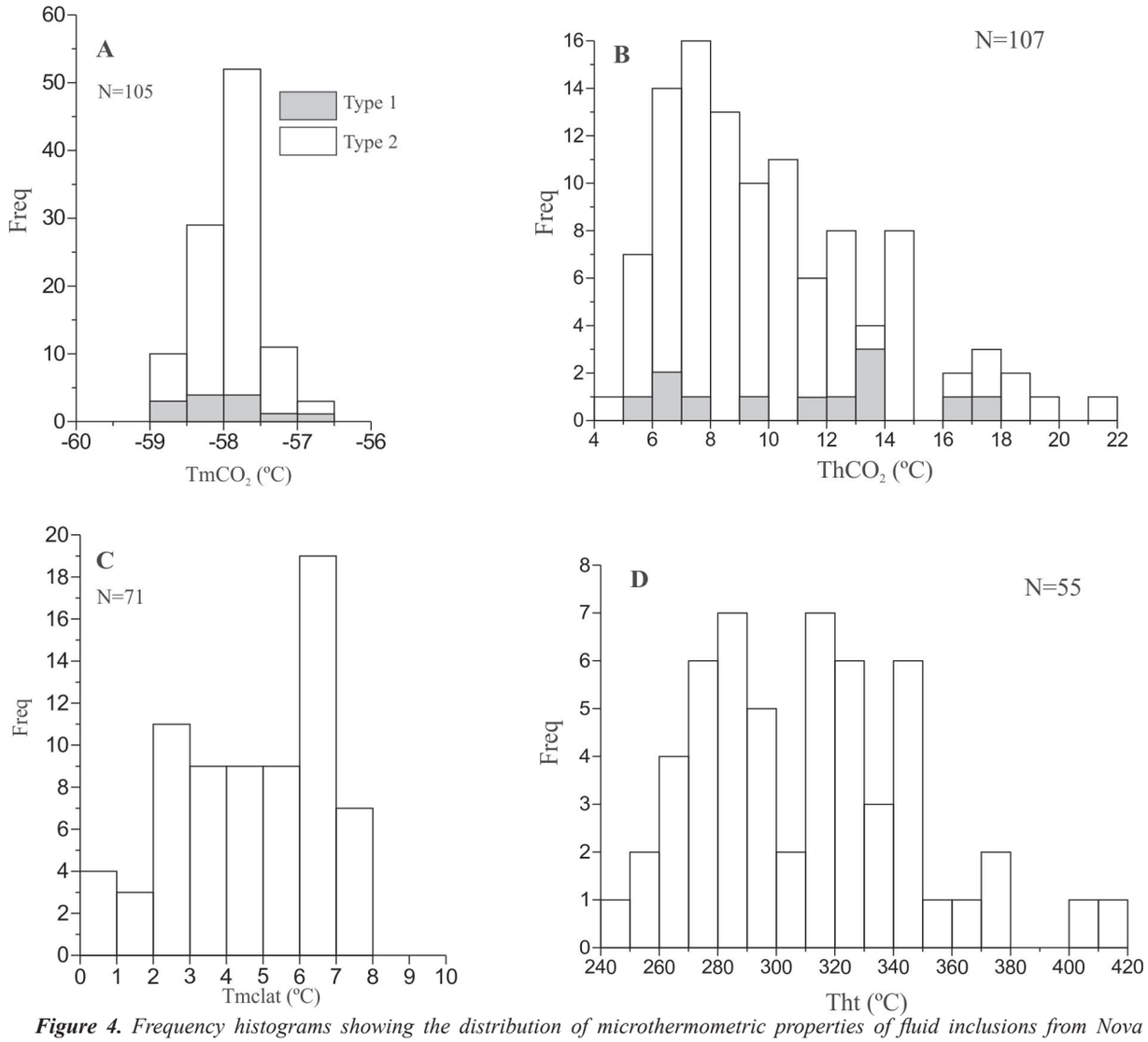

Figure 4. *Frequency histograms showing the distribution of microthermometric properties of fluid inclusions from Nova Esperança.*

Figura. 4. *Histogramas de frequência mostrando a distribuição das propriedades microtermométricas das inclusões fluidas em Nova Esperança.*

is generally less than 5°C; a few clusters show 9-16°C internal differences. This may suggest pressure fluctuation. Furthermore, the asymmetric distribution of $ThCO_2$ (Fig. 4B) is compatible with fluid immiscibility (e.g., Loucks 2000).

The frequency distribution of Th shows large variation and two poorly defined peaks at 290° and 320°C (Fig. 4D). Again this may represent a combination of fluid immiscibility and necking down, with main trapping occurring at 290°C, which is similar to what occurred at Divisão, although vertical trends are not present in this case. Pressure estimates are in the range of 1.6-2.5kbar.

Mamão - Two veins of the Mamão deposit have been investigated (samples 81A and 81D, about 150 studied fluid inclusions). The quartz veins show cataclastic fabric with large irregular crystals and fragments of crystals showing moderate to strong undulose extinction. Swarms of fluid inclusions cut across the crystals with irregular to elongate and negative crystal shapes, and sizes ranging from 5 to 20 dm (mostly around 10dm). These inclusions are secondary, and few inclusions occur in randomly distributed clusters or trails. Some show evidence of necking down. The volume of the carbonic phase spread between 25-95% (mostly 35-55%).

The different types of fluid inclusions show similar, although not identical, distribution, relationships, and microthermometric properties in distinct veins. Type 2 predominates over Types 1 and 3. $TmCO_2$ in Types 1 and 2 occurred between -57.4° and -61.1°C. The frequency distribution is asymmetric with the histogram skewed to the right showing a modal value of -57.5°C.

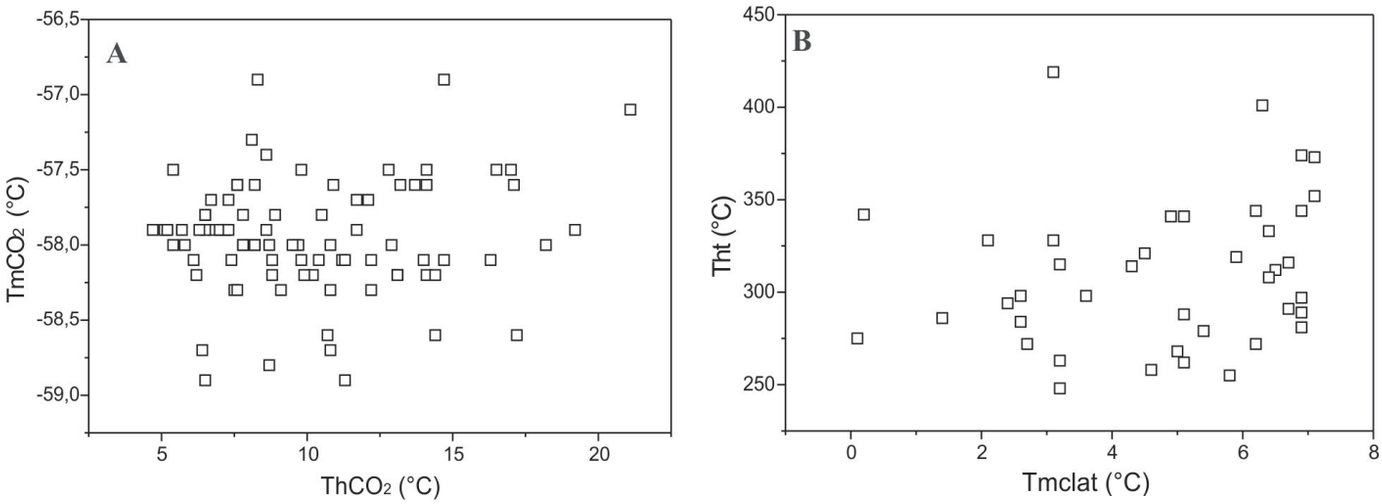

Figure 5. A) *ThCO2 x TmCO2 and B) Tmclat x Th relationships of fluid inclusions from Nova Esperança.*
Figura 5. A) *relações entre A) ThCO2 x TmCO2 e B) Tmclat x Th em inclusões fluidas de Nova Esperança.*

Also, values lower than -58.3°C are restricted to sample 81D (Fig. 6A). These results indicate the large predominance of CO_2 in the carbonic phase. Micro-Raman analyses, however, detected only trace amounts of CH_4 (Table 1), and a shift at about 2950 cm^{-1} that may correspond to C_2H_6 (Burke, 1991). The partial homogenization of the carbonic phase shows a normal, nearly symmetric, distribution, ranging from 7.0° to 26.0°C and a peak at 19.0°C (Fig. 6B).

Clathrates in Type 2 inclusions melted between 5.7° and 10.6°C in sample 81D and in a very narrow range, between 7.6° and 8.2°C in sample 81A (Fig. 6C). The modal value in sample 81D is 8.2°C, which imply nearly the same salinity of about 3.2 wt. % NaCl equiv. for the two samples. The values higher than 10°C found in sample 81D reflect the presence of CH_4 in some inclusions (Collins 1979).

The final homogenization of Type 2 inclusions occurred in similar ranges in the two samples: 261°-350°C (mode at 305°C) and 300°-390°C (mode at 335°C) for samples 81A and 81D, respectively (Fig. 6D). It is noteworthy that only two, out of 57 investigated fluid inclusions, homogenized to the liquid phase.

In aqueous Type 3 inclusions Tmice occurred in a narrow range of -3.9° and -5.3°C in both samples, indicating salinities of 6.3-8.1 wt. % NaCl equivalent. Eutectic temperatures were observed only in sample 81D and recorded in the range of -33.9° and -38.6°C, suggesting that this fluid belong to the H_2O-NaCl-$MgCl_2$ (or $FeCl_2$) system (Borisenko 1977). In this type, Th occurred between 179° and 259°C in sample 81A, and between 60° and 112°C in sample 81D (Fig. 6D), clearly showing fluids trapped in different temperatures.

DISCUSSION

The fluid inclusion results of the Mamão deposit reveal complexities with respect to the processes that generated the inclusions in that contrasting explanations arise from the data. The nearly symmetrical frequency distribution of $ThCO_2$ (Fig. 6B) indicates necking down of fluid inclusions trapped from a homogeneous fluid in the one-phase field of the T-P space (i.e., this is not necking down induced by deformation, Loucks 2000). This is favored by the little variation observed in the salinity and $TmCO_2$ values and the absence of correlation between $TmCO_2$ and $ThCO_2$ and between Tmclat and Th (Fig. 7A). On the other hand, vertical trends in the Tmclat versus Tht space (Fig. 7B) indicate leakage.

The final homogenization shows a relatively narrow interval of values, spreading <90°C within a vein, but with variations of 10°-55°C within single clusters or trails.

Previously studied deposits - Data from the Serra do Ipitinga occurrence have been presented elsewhere by Faraco *et al*. (2006) and data from the Carará deposit will be discussed in details in Klein & Fuzikawa (in preparation). These data are only summarized here.

SERRA DO IPITINGA - Faraco *et al*. (2006) conducted a fluid inclusion study in a sheared quartz vein from Serra do Ipitinga. The authors identified three types (and three sub-types) of aqueous inclusions that show variable salinities, from 0.6 to 28wt. % of NaCl or $CaCl_2$ equiv., and trapping temperatures that spread from 100° to 230°C. These data have been interpreted in terms of mixing of aqueous fluids of distinct temperature and salinities, and the quartz vein has been considered to belong to the class of orogenic gold deposits. It is worth noting that neither

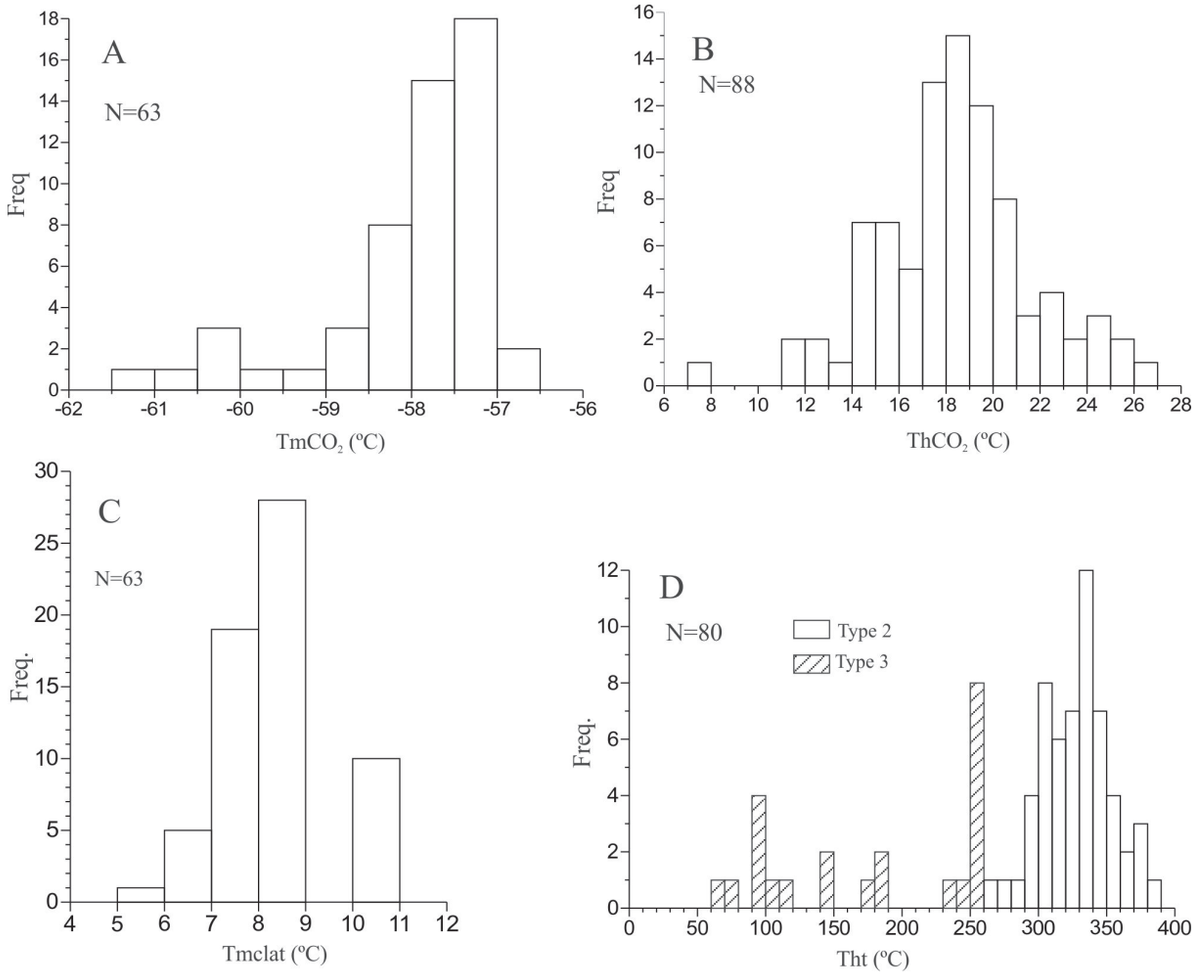

Figure 6. *Frequency histograms showing the distribution of microthermometric properties of fluid inclusions from Mamão.*
Figura 6. *Histogramas de frequência mostrando a distribuição das propriedades microtermométricas das inclusões fluidas em Mamão.*

the chemical systems, characterized by the absence of CO_2, nor the temperature range are usually found in the class of lode gold or orogenic deposits (see reviews in Groves *et al*. 2003, McCuaig & Kerrich 1998). The data are also distinct from those found in all other deposits of the Ipitinga Auriferous District.

CARARÁ - The fluid system of the Carará deposit constitutes a peculiar case. Nearly all fluid inclusions are dark one-phase carbonic inclusions that belong to Type 1 described above. Only seven, out of 250 investigated fluid inclusions are two-phase aqueous-carbonic inclusions (Type 2). Furthermore, this subordinate population is restricted to the tourmaline-rich vein.

The melting of CO_2 in both carbonic and aqueous-carbonic types occurred between –56.6ºC and –58.2ºC, with a sharp peak at –57.4ºC. This indicates that only subordinate amounts of other volatiles could be dissolved in the CO_2 fluid, which was confirmed by the micro-Raman spectroscopic analysis that identified only small proportions (< 2%) of N_2. The homogenization of the carbonic phase of the Type 1 inclusions occurred between -28.5ºC to 29.9ºC, with most of the values clustering between 2ºC and 10ºC. In Type 2 fluid inclusions $TmCO_2$ values were recorded mostly at -57.7°C. The $ThCO_2$ occurred between 23.5ºC and 26.5ºC, and clathrates melted between 7.2ºC and 7.6ºC, indicating salinities around 5wt%NaCl equivalent. The final homogenization (to liquid) occurred in the range of 264º-346ºC.

STABLE ISOTOPES

A reconnaissance stable isotope study was carried out especially in quartz samples of seven deposits. Muscovite and tourmaline samples of the Carará and Catarino deposits were also analyzed. The results are presented in Table 2 and Figure 8. Regionally, the quartz samples show a fairly restricted range of $\delta^{18}O$ values between +10.6 and +13.9‰ (Fig. 8A). Within a single deposit, however, variations are generally less than 1‰.

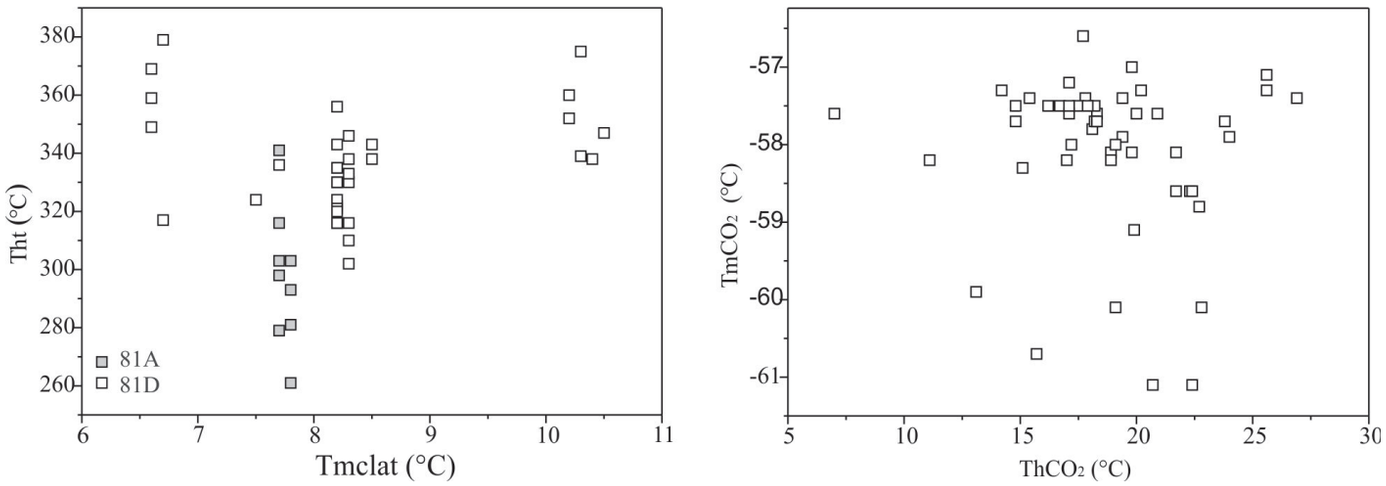

Figure 7. A) *ThCO2 x TmCO2 and B) Tmclat x Th relationships of fluid inclusions from Mamão.*
Figura 7. A) *relações entre A) ThCO2 x TmCO2 e B) Tmclat x Th em inclusões fluidas de Mamão.*

Exceptions are the quartzite-hosted veins at Catarino and Carará that show internal variations of 1.3‰ and 2.1‰, respectively. A brief discussion for individual deposits is presented below, together with fluid composition estimated from the measured isotopic values and using appropriate isotope fractionation equations and relevant temperatures (Table 3).

Divisão - One quartz sample was analyzed at Divisão. This sample has a $d^{18}O$ value of +11.3‰, which combined with fluid inclusion homogenization temperatures (~290°C) gives a fluid $d^{18}O$ value of +4.1‰. This composition is compatible with a metamorphic source, but it is not far off the magmatic field.

Nova Esperança - Samples of quartz from two veins gave $d^{18}O$ values of +12.9 and +13.9‰. Fluids extracted from fluid inclusions in these same samples yielded dD values of -76 and -43‰, respectively, and CO_2 $d^{13}C$ values of -4.6 and 0.0‰, respectively.

The $d^{18}O$ fluid compositions estimated from measured isotope values and fluid inclusion homogenization temperatures (290°-320°C) fall between +5.7‰ and +7.7‰. Combined fluid $d^{18}O$ values with the dD values of fluid inclusion waters are compatible with both magmatic and metamorphic sources for the fluid (Fig. 9). The more negative $d^{13}C$ value from inclusion CO_2 indicate deep-seated sources that might be mantle, metamorphic or magmatic in origin. The value of 0‰ is compatible with seawater and marine carbonates. Seawater remains a possible source, and carbonate rocks are not known in the study area.

Igarapé do Inferno - The quartz from igarapé do Inferno shows a $d^{18}O$ value of +13.9‰. No external temperature information is available for this deposit. However, considering the regional similarity among the studied gold-quartz vein deposits, a value of 300°C is assumed, which gives a fluid $d^{18}O$ value of +7.0‰ for this deposit. This value is in accord with both magmatic and metamorphic sources.

Table 3. *Isotopic composition of the fluid in equilibrium with hydrothermal minerals of gold deposits from the Ipitinga Auriferous Distric.t*
Tabela 3. *Composição isotópica do fluido em equilíbrio com minerais hidrotermais de depósitos auríferos do Distrito Aurífero de Ipitinga.*

deposit	T (°C)	mineral	$\delta^{18}O_{H2O}$ (‰)	δD_{H2O} (‰)
Divisão	290	quartz	+4.1	
Nova Esperança	290-320	quartz	+5.7 - +6.7	-76
	290-320	quartz	+6.7 - +7.7	-43
Igarapé Inferno	300	quartz	+7.0	
Mamão	305-335	quartz	+5.9 - +6.9	-49
	305	quartz	+6.8 - +7.8	-75
	305	quartz	+6.2 + 7.2	-58
	305	quartz	+6.2 + 7.2	-62
Castanhal	300	quartz	+6.1	-66
	300	quartz	+5.7	
Limão	300	quartz	+7.0	
	300	quartz	+6.3	-60
	300	quartz	+6.2	-51
	300	quartz	+6.5	
Catarino	305	quartz	+5.3	
	305	tourmaline	+7.7	
	305	muscovite	+6.7	-30
	305	quartz	+4.3	
	305	quartz	+4.5	
	305	muscovite	+7.4	-47
	305	muscovite	+6.4	-45
Carará	346	quartz	+6.4	
	346	quartz	+7.0	
	346	tourmaline	+8.3	-34
	346	muscovite	+7.0	-20
	346	quartz	+6.6	-33
	346	quartz	+7.3	
	346	quartz	+5.6	-61
	346	quartz	+5.2	
	346	tourmaline	+7.5	-28

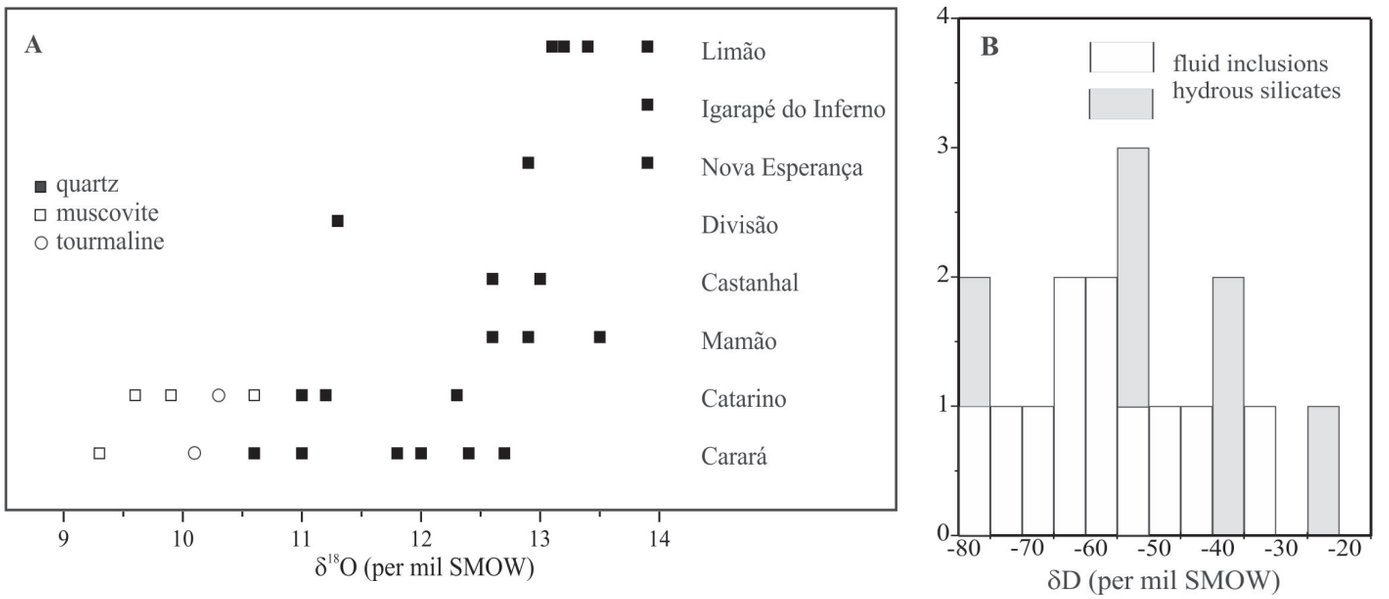

Figure 8. A) *Mineral δ18O values from gold deposits. B) Frequency histogram of mineral and fluid inclusion δD values from gold deposits.*
Figura 8. A) *Valores de δ18O em minerais. B) Histograma de frequência com a distribuição dos valores de δD em minerais e inclusões fluidas.*

Mamão - Quartz from four different veins at Mamão shows a relatively narrow range of $d^{18}O$ values, from +12.6 to + 13.5‰ (Fig. 8A, Table 2). The dD values measured in inclusion fluids from these same four vein quartz samples spread between -49 and -75‰ (Fig. 8B).

Estimation of fluid compositions derived from quartz analyses in the fluid inclusion homogenization temperature interval of 305°-335°C gave $d^{18}O$ values of +5.9 to +7.8‰. These values, combined with the hydrogen isotope compositions of inclusion fluid waters are consistent with both magmatic and metamorphic sources for the mineralizing fluids (Fig. 9). The fluid CO_2 detected in inclusion fluids of one of the quartz samples gave a $d^{13}C$ value of -2.7‰, which is compatible with mantle, magmatic or metamorphic sources.

Castanhal - Two quartz veins from Castanhal show d18O values in quartz of +13.0 and +12.6‰. In the absence of external geothermometer, a possible temperature of 300°C is assumed, which gives fluid d18O values of +5.7 to +6.1‰. These values, combined with the dD value of -66‰ obtained in fluid inclusion waters are in keeping with both magmatic and metamorphic source for the fluid (Fig. 9).

A strongly negative d13C value of -30.2‰ was measured in fluid inclusion CO2. This value clearly indicates an organic origin for the carbon present in the inclusions.

Limão - Four quartz samples from Limão furnished a narrow range of $d^{18}O$ values, from +13.1 to +13.9‰, despite the distinct textural and structural aspects of the veins. This data suggests that deformation has not affected the oxygen isotope

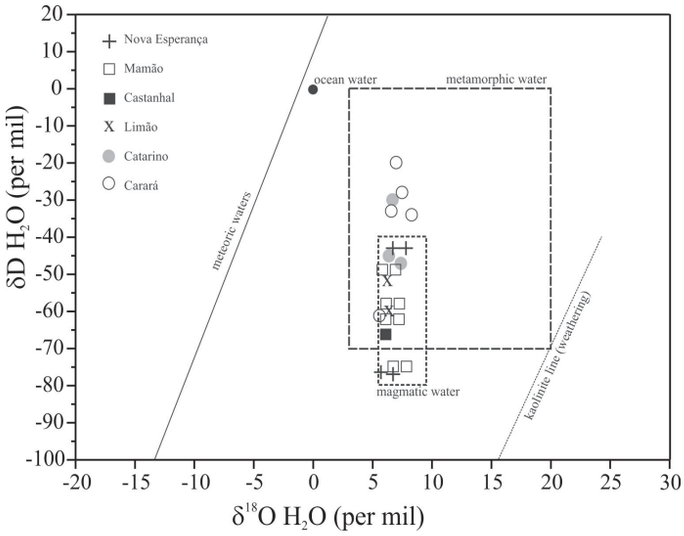

Figure 9. *Oxygen and hydrogen isotope composition of the water in equilibrium with minerals and fluid inclusions of gold deposits from the Ipitinga Auriferous District in relation to the primary magmatic and metamorphic water fluids, as defined by Sheppard (1986).*

Figura 9. *Composição dos isótopos de oxigênio e hidrogênio da água em equilíbrio com minerais e inclusões fluidas em depósitos do Distrito Aurífero de Ipitinga em relação aos campos de fluidos magmáticos primários e metamórficos, conforme definição de Sheppard (1986).*

Catarino - At Catarino, three quartz samples show $d^{18}O$ values between +11.0 and +12.3‰. A tourmaline sample has a $d^{18}O$ value of 10.3‰, and muscovite shows $d^{18}O$ values between +9.6 and +10.6‰ and δD values between -38 and -55‰ (Table 2, Fig. 8).

Applying the oxygen isotope fractionation equation of Chacko *et al*. (1996) for the quartz-muscovite pair, temperatures of 447° and 630°C are obtained. Also, the quartz-tourmaline pair gives a temperature of 515°C using the fractionation factors of Kotzer *et al*. (1993). These temperatures are apparently high, when compared with fluid inclusion homogenization temperatures found in other deposits of the same district and with mineralogical constraints, such as the presence of muscovite in the alteration and absence of a higher-temperature mica (biotite). However, without an external geothermometer and since the isotopic pairs have not yielded consistent temperatures, the formation conditions and fluid composition at Catarino remain uncertain. Assuming a mean value of 305°C from range of fluid inclusion homogenization temperature of the similar and nearby Carará deposit (see below), $\delta^{18}O$ values of +4.3 to +7.3‰, +6.4 to +7.4‰, and +7.7‰ have been obtained for fluids in equilibrium with quartz, muscovite, and tourmaline, respectively (Table 3). In addition, fluid δD values of -30 to -47‰ have been estimated from muscovite. These results mostly overlap the fields of magmatic and metamorphic waters (Fig. 9).

Carará - At Carará, samples have been taken from the high-grade quartz (80A - HGQ), low-grade quartz (80C - LGQ), and the barren tourmaline-rich vein (80B - TRV). The $\delta^{18}O$ values of quartz from the high- and low-grade quartz are similar, although not identical (+11.8 to +12.4‰ and +12.0 to +12.7‰, respectively), while they are lower in the tourmaline-rich vein (+10.6 to +11.0‰). Inclusion fluid waters yielded δD values of -33 and -61‰ in the LGQ and TRV, respectively. No water has been detected in fluid inclusions from the HGQ (see fluid inclusion section). Carbon CO_2 in the fluid inclusions gave ^{13}C values of -3.4‰, -3.2‰, and -14.6‰ in the HGQ, LGQ, TRV, respectively (Table 2). These results indicate similar isotopic compositions for the HGQ and LGQ, which are, in turn, rather distinct from the compositions found in the barren TRV.

One sample of muscovite of the HGQ gave a $\delta^{18}O$ value of +9.3‰ and δD value of -38‰. Tourmaline of the same vein gave $\delta^{18}O$ and δD values of +10.1‰ and -77‰, respectively, whereas in the TRV the $\delta^{18}O$ and δD values are in tourmaline are +9.3‰ and -71‰, respectively.

Oxygen isotope thermometry was applied, using the quartz-tourmaline fractionation factor of Kotzer *et al*. (1993), and the quartz-muscovite fractionation factor of Chacko *et al*. (1996). Obtained values are within the range of 775°-600°C for the quartz-tourmaline pairs in the HGQ and TRV, and is 475°C for the quartz-muscovite pair of the HGQ. These values are unrealistically high when compared with the structural and metamorphic characteristics of the deposit, with the alteration mineralogy, and with the homogenization temperatures of scarce aqueous-carbonic fluid inclusions found in the TRV (264-346°C). Accordingly, the temperature of the ore- bearing fluid is likely to have been within the range of the fluid inclusion homogenization temperatures. This indicates that the mineral pairs may have not deposited in equilibrium. Alternatively, they may have undergone isotope change after crystallization.

At the temperature of 346°C, the $\delta^{18}O_{H2O}$ values calculated from quartz range from 6.4 to 7.0‰ in the mineralized veins (HGQ, LGQ), and from +5.2 to +5.6‰ in the barren TRV. The values calculated from tourmaline and muscovite are in the range of 7.0 to 8.3‰. δD_{H2O} values of inclusion fluids are -33‰ in the LGQ and -61‰ in the barren TRV, and those calculated from hydrous silicates vary between -20 and -34‰. These values consistently indicate metamorphic sources for the fluids at Carará (Fig. 9).

RADIOGENIC ISOTOPES

Pb Isotopes - Lead isotope compositions were determined in sulfide samples from Divisão, igarapé do Inferno and Limão. The results are presented in Table 4. The pyrite and galena concentrates from Divisão show similar compositions, but the pyrite sample is slightly more radiogenic than the galena samples. All analyses from Divisão plot close to the orogen growth curve in both uranogenic and thorogenic diagrams (Fig. 10) of Zartman & Doe (1981). However, in the uranogenic diagram the galena samples plot below the orogen curve, whereas the pyrite sample plot above this curve, and both diagrams show absence of significant contribution of lower crustal sources (Fig. 10A). Model ages calculated according to the two-stage model of Stacey & Kramers (1975) gave values of 2106, 2113 and 2122Ma for galena samples and 2183Ma for pyrite (Table 5).

The Pb isotope composition of pyrite concentrates from the igarapé do Inferno and Limão deposits are quite different and more radiogenic than those from Divisão. These compositions plot above the orogen (igarapé do Inferno) and below the upper crust (Limão) evolutionary curves in the uranogenic diagram of Zartman & Doe (1981) (Fig. 10A). In the thorogenic diagram both values plot approximately on the orogen curve (Fig 10B). Model ages calculated according to the two-stage model of Stacey & Kramers (1975), yield values of 1774Ma for igarapé do Inferno, and 1902Ma for Limão (Table 5).

$^{40}Ar/^{39}Ar$ isotopes - Ar isotopes analyses were performed in muscovite crystals from the high-grade quartz vein of the Carará (sample EK80) deposit and a quartz vein from the Catarino (sample EK106M1) deposit. Two grains from Carará produced plateau ages (1940±30 and 1950±30Ma) that are compatible at the 2-sigma confidence level. The step-heating spectrum (Fig. 11A) indicates a single gas reservoir with minor loss of Ar from the least retentive sites for one of the grains. The age-probability spectrum, plotted for all the steps of both grains, is shown in the age probability plot as a dashed line (Fig. 11B). The age-probability spectrum of only the plateau steps of the two grains is shown by the solid line in the plot and yields a maximum probability peak at 1950Ma and a mean weighted age

of 1940 ± 20 Ma which is compatible at the 2-sigma level with the ages given by the plateaus (1940±30 and 1950±30Ma). The mean weighted age of 1940±20 Ma is the best estimate for this sample's age.

Two grains from Catarino produced plateau ages (1900±30 and 1940±30Ma) that are compatible at the 2-sigma confidence level. The step-heating spectrum (Fig. 11C) indicates a single gas reservoir with minor loss of Ar from the least retentive sites. The age-probability spectrum plotted for all the steps of both grains is shown in the age probability plot as a dashed line (Fig. 11D). The age-probability spectrum of only the plateau steps of the two grains is shown by the solid line in the plot and yields a maximum probability peak at 1946Ma and a mean weighted age of 1930±20 Ma, which is compatible at the 2-sigma level with the ages given by the plateaus (1900±30Ma and 1940±30 Ma). The mean weighted age of 1930±20 Ma is a suitable estimate for the age of this sample.

Table 4. *Lead isotope compositions of sulfide minerals from gold deposits of the Ipitinga Auriferous District.*
Tabela 4. *Composição isotópica do Pb em sulfetos de depósitos auríferos do Distrito Aurífero de Ipitinga.*

deposit	sample	mineral	$^{206}Pb/^{204}Pb$	σ	$^{207}Pb/^{204}Pb$	σ	$^{208}Pb/^{204}Pb$	σ	model age (Ma)*
Divisão	78C	pyrite	15.049	0.009	15.250	0.013	34.946	0.042	2183
	78C1	galena	14.983	0.012	15.161	0.018	34.700	0.055	2106
	78C2	galena	14.998	0.012	15.181	0.018	34.760	0.055	2122
	78C3	galena	14.991	0.012	15.171	0.018	34.730	0.055	2113
Limão	79B	pyrite	15.762	0.010	15.453	0.014	35.358	0.043	1902
Igarapé do Inferno	178	pyrite	15.875	0.010	15.426	0.014	35.537	0.043	1774

**Calculated according to the two-stage model of Stacey and Kramers (1975)*

Table 5. *Relevant geochronological data for the Ipitinga Auriferous District.*
Tabela 5. *Sumário de dados geocronológicos para o Distrito Aurífero de Ipitinga.*

rock type	unit / location	dated material	crystallization age (Ma)	metamorphic age (Ma)	Pb-Pb model age (Ma)	$^{40}Ar/^{39}Ar$ age (Ma)	Ref.
mafic metavolcanic rock	Ipitinga Group	whole rock	2265 ± 34[b]				1
monzogranite	undivided orogenic granites	zircon	2177 ± 3[a]				2
Diorite	Carecuru Intrusive Suite	zircon	2140 ± 1[a]				3
muscovite-garnet-granite	syn-tectonic granite	zircon	2030 ± 2[a]				2
anorogenic granite	Waiãpi Granite	zircon	1753 ± 3[a]				4
		monazite		2038 ± 6[c]			5
Diorite	Carecuru Intrusive Suite	amphibole				2074 ± 17	6
Diorite	Carecuru Intrusive Suite	biotite				1928 ± 9	6
Diorite	Carecuru Intrusive Suite	biotite				1833 ± 13	6
quartz vein	Carará deposit	muscovite				1940 ± 20	7
quartz vein	Catarino deposit	muscovite				1930 ± 20	7
quartz vein	Igarapé do Inferno deposit	pyrite			1774		7
quartz vein	Limão deposit	pyrite			1902		7
quartz vein	Divisão deposit	galena			2106		7
quartz vein	Divisão deposit	galena			2122		7
quartz vein	Divisão deposit	galena			2113		7
quartz vein	Divisão deposit	pyrite			2183		7

a – Sm-Nd isochron, b – Pb-evaporation
Key to references 1 – McReath & Faraco (2006), 2 – Rosa-Costa et al. (2006), 3 – Rosa-Costa et al. (2003), 4 – Vasquez & Lafon (2001), 5 – Rosa-Costa et al. (i n pressA), 6 – Rosa-Costa et al. (in pressB), 7 – this study

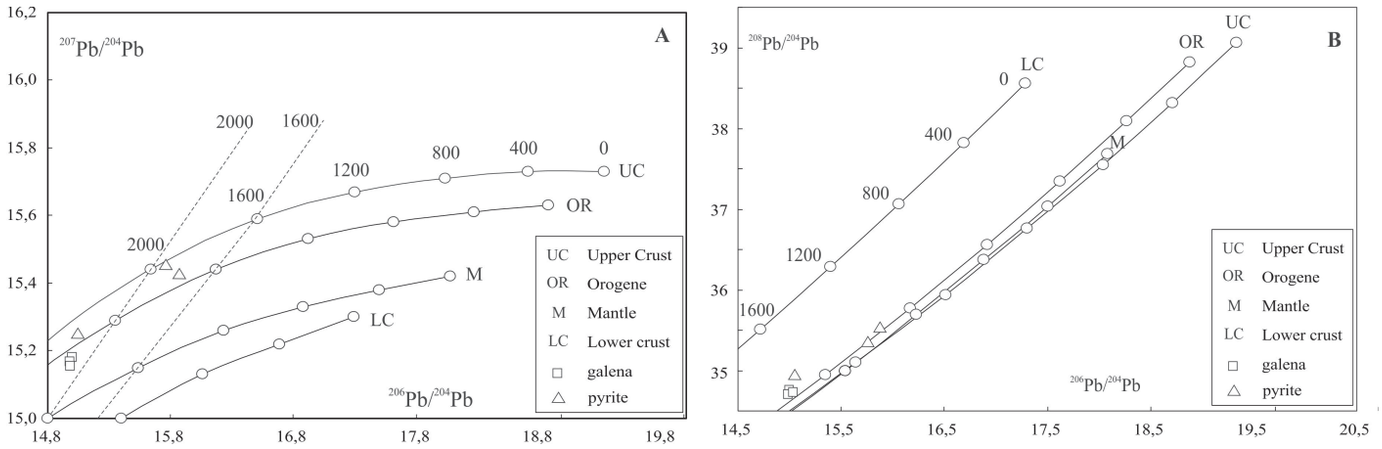

Figure 10. *Pb isotope composition of sulfide minerals associated with gold deposits of the Ipitinga Auriferous District. The growth curves are those from Zartman & Doe (1981).*

Figura 10. *Composição isotópica do Pb em sulfetos associados a depósitos auríferos do Distrito Aurífero de Ipitinga em relação às curvas evolutivas de Zartman & Doe (1981).*

Interpretation of the radiogenic isotope data - Geologic evidence strongly indicates that gold mineralization in the Ipitinga Auriferous District is post-metamorphic and that it is synchronous and/or slightly younger with respect to the development of strike-slip shear zones at the boundary between the Carecuru and Jari domains (Klein & Rosa-Costa 2003). The timing of this structural event is constrained by the intrusion of muscovite- and/or garnet-bearing crustal granites at 2030±2 Ma (Rosa-Costa *et al*. 2006), whereas monazite ages constrained the metamorphism at about 2038±6Ma (Rosa-Costa *et al*. in pressA). Thus, the time interval of 2038-2030Ma is interpreted to be the upper limit for the gold mineralization.

Rosa-Costa *et al*. (in pressB) provided $^{40}Ar/^{39}Ar$ ages in amphibole and biotite from calc-alkaline diorites of the Carecuru Intrusive Suite (2140±1Ma, single zircon Pb-evaporation age). This suite is closely associated with, and hosts part of, gold mineralization in the Ipitinga District (Fig. 1). The amphibole yielded an age of 2074±17Ma, and biotite gave ages of 1928±9Ma and 1833±13Ma. Rosa-Costa *et al*. (in press B) interpreted the amphibole data as the result of low cooling rates from emplacement to closure of the isotopic system, whereas the biotite ages have been interpreted to reflect post-crystallization isotopic resetting induced by a thermal event associated with the emplacement of anorogenic granitoids at 1.88-1.86Ga. Considering the K-Ar blocking temperature of 375±50°C for muscovite (Quigley *et al*. 2006), it is possible that the $^{40}Ar/^{39}Ar$ muscovite ages of 1930-1940 Ma obtained in our study also reflect the regional cooling or, alternatively, the anorogenic event and not the age of gold mineralization, although plutons of this magmatic event are not known to date in the Carecuru domain. Therefore, the Ar ages are only minimum ages for the gold mineralizing episode, which is then bracketed between 2030 and 1940Ma.

The Pb-Pb model ages calculated from pyrite and galena from the Divisão deposit are quite different. The pyrite age is older than the age of the hosting granitoids (~2.14Ga) and the isotopic composition is product of mixed sources or from older (~2.26Ga) Paleoproterozoic sources (e.g., Mcreath and Faraco 2006, Rosa-Costa *et al*. 2006). Although quite younger, the consistent galena ages are also older than the upper time limit for mineralization estimated from the metamorphic ages. Therefore, the dated galenas may also indicate mixed (upper crust and mantle) sources.

In the igarapé do Inferno deposit the obtained Pb-Pb model age (1774 Ma) is much younger than the 1928±9Ma and 1833±13Ma $^{40}Ar/^{39}Ar$ biotite age reported by Rosa-Costa *et al*. (in pressB). The model age is similar to the age of the anorogenic magmatism (Vasquez and Lafon 2001). It could be possible that the sulfides incorporated a younger, radiogenic Pb from this thermal event. An upper crustal Pb source is inferred for this deposit. The Pb-Pb model age of 1902Ma calculated for the Limão deposit also falls off the possible time window for gold mineralization in the district and an upper crustal Pb source is also suggested by the isotopic results.

DISCUSSION AND CONCLUDING REMARKS

Interpretations of fluid composition for Castanhal, Limão and Catarino rely on assumed temperatures because geothermometric information is lacking for these deposits. Notwithstanding, the estimated compositions are in good agreement with those calculated for better constrained deposits (Nova Esperança, Mamão and Carará). Fluid inclusion

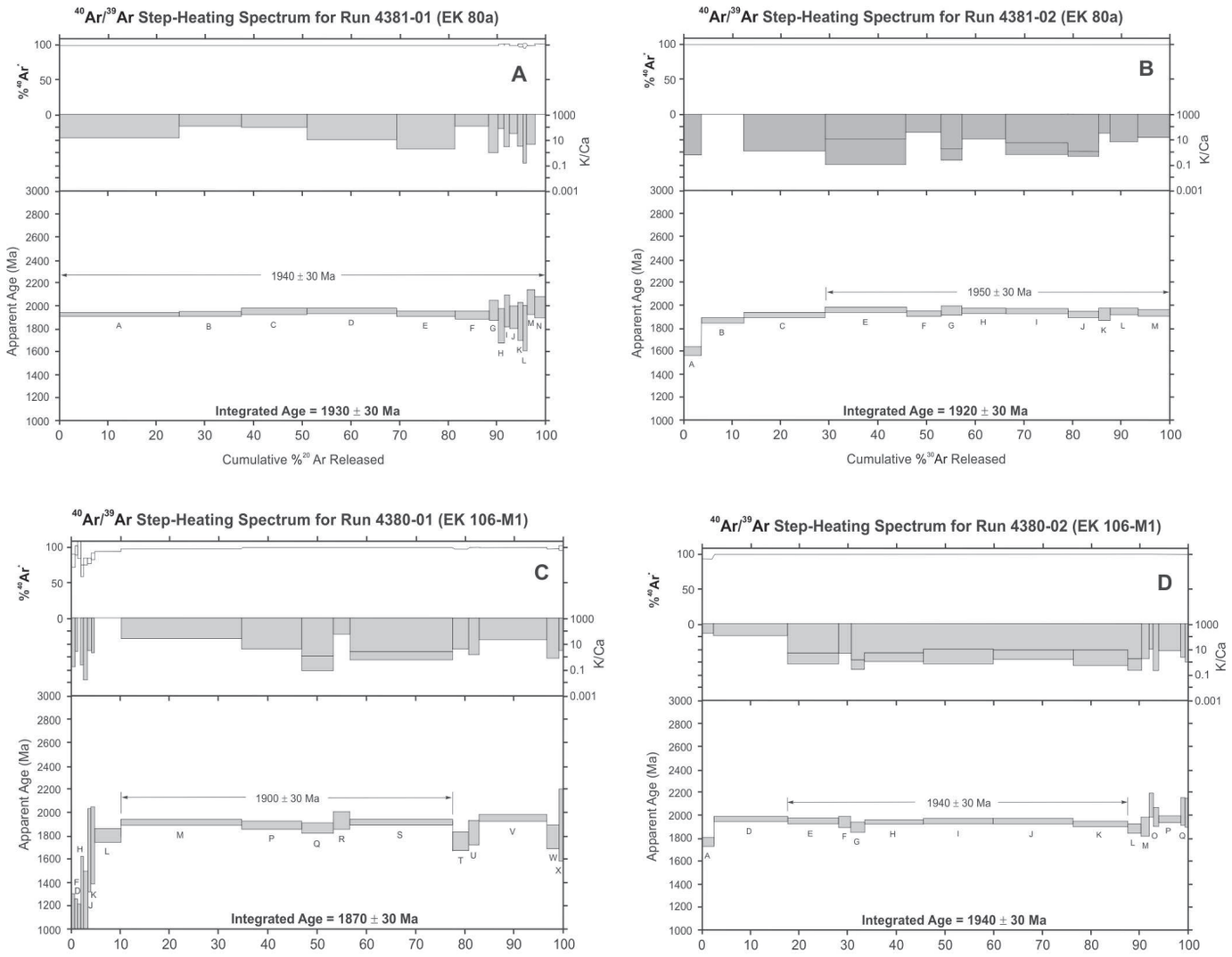

Figure 11. *$^{40}Ar/^{39}Ar$ plots for muscovite analyses from Carará and Catarino. A) Step-heating spectrum from Carará. B) Age-probability spectrum from Carará. C) Step-heating spectrum from Catarino. D) Age-probability spectrum from Catarino.*

Figura 11. *Diagramas com resultados $^{40}Ar/^{39}Ar$ em muscovita dos depósitos Carará e Catarino. A) Espectro do aquecimento gradual em Carará. B) Espectro da probabilidade de idade em Carará. C) Espectro do aquecimento gradual em Catarino. D) Espectro da probabilidade de idade em Catarino.*

compositions and temperatures are in keeping with a metamorphic origin for the aqueous-carbonic fluids (Phillips & Powell 1993) in the investigated deposits, except for the Serra do Ipitinga showing described by Faraco *et al*. (2006). Oxygen and hydrogen isotopes show that at Mamão, Castanhal, Limão and Catarino deposits fluid compositions fall in the field of magmatic waters, and that they mostly overlap the metamorphic field. Carará shows a distinct behavior in that the calculated compositions, with one exception, plot in the metamorphic field (Fig. 9). Lead isotope compositions of sulfides from three deposits are compatible with mixed mantle and crustal sources.

In addition to the relative timing of ore formation (in relation to magmatism, metamorphism, and deformation), the absolute timing is critical for modeling gold deposition. Geologic evidence indicates that the gold mineralizing event is slightly younger than 2038-2030Ma and older than the muscovite ^{40}Ar-^{39}Ar ages of 1930-1940Ma. Although our radiogenic data could not constrain the absolute age of the ore-forming event, the relative timing is compatible with the presence of both magmatic and metamorphic hydrothermal systems at that time.

Metamorphic fluids may be produced by devolatilization and dehydration reactions during the prograde metamorphism of volcanossedimentary sequences, at moderate crustal depths (12-18km), as the result of tectonic thickening caused by collision (Kerrick & Caldera 1998). The low salinities would arise from the metamorphism of sequences deposited in

oceanic and accretionary settings (Yardley & Graham 2002). This is consistent with the orogenic scenario proposed for the Carecuru and Jari domains in Paleoproterozoic times (Rosa-Costa *et al.* 2006).

The origin of the CO_2-only fluid inclusions at Carará, which clearly show a metamorphic signature, is still uncertain and subject of ongoing research (Klein & Fuzikawa in preparation). Possible origins that are under discussion include: (1) selective water leakage induced by plastic deformation of the host quartz, (2) selective entrapment of CO_2 following the unmixing of a H_2O-CO_2 fluid, (3) existence of a true CO_2-transporting fluid.

Potential sources for magmatic fluids are the syn-tectonic granitoids of c.a. 2030Ma. In general, a granitic signature involves the presence of high-temperature (>450°C), high-salinity (>25wt.%NaCl) aqueous fluid inclusions, and more oxidizing conditions (Roedder 1992), which is not the case here. On the other hand, low-salinity aqueous-carbonic fluids may be produced by felsic hydrothermal systems under special conditions. These include magmas produced at depth, with pressures in excess of 3 kb, because of the limited solubility of CO_2 in felsic magmas at low pressures, and special relationships between CO_2-H_2O and chlorine (Roedder 1992, Lowenstern 2001, Baker 2002).

The carbon isotopes of inclusion fluids show two contrasting groups of $d^{13}C$ values: 0.0 to -4.6‰ and -25.5 to -30.2‰. The latter values clearly indicate organic contribution. This could be reflective either of devolatilization in a sequence having a large contribution of biogenic carbon or contamination of the CO_2-bearing fluid at the site of trapping. The slightly depleted values, however, do not provide a single source for the carbon, since mantle- magmatic- and metamorphic-derived carbon present similar range of values (McCuaig & Kerrich 1998).

As a whole, the vein quartz gold deposits of the Ipitinga District are consistent with the class of orogenic gold deposits (Groves *et al*., 2003), although multiple processes and sources are permissive for the studied deposits. With respect to the Serra do Ipitinga showing, it must be considered the hypothesis that this showing does not belong to the class of orogenic deposits as stated by Faraco *et al*. (2006). The fluid properties determined by those authors are not easily found in the proposed class (see exhaustive reviews in McCuaig & Kerrich 1998, Groves *et al*. 2003, Goldfarb *et al*. 2005). Alternatively, this showing might represent a gold-bearing vein associated with the volcanogenic-style copper mineralization discussed by Faraco *et al*. (2006).

Acknowledgments - The authors thank Dr. Hilton Tulio Costi for the review of the manuscript. Dr. Kazuo Fuzikawa is thanked for providing the micro-Raman data. The senior author acknowledges the Conselho Nacional de Desenvolvimento Científico e Tecnológico (CNPq) for a research grant (process 306994/2006-0).

References

Baker T. 2002. Emplacement depth and carbon dioxide-rich fluid inclusions in intrusion-related gold deposits. *Economic Geology*, **97**: 1111-1117.

Borisenko A.S. 1977. Study of the salt composition of solutions in gas-liquid inclusions in minerals by the cryometric method. *Soviet Geol. & Geophys*., **18**: 11-19.

Bowers T.S. & Helgeson H.C. 1983. Calculation of the thermodynamic and geochemical consequences of nonideal mixing in the system H_2O-CO_2-NaCl on phase relations in geologic systems: equation of state for H_2O-CO_2-NaCl fluids at high pressures and temperatures. *Geochimica et Cosmochimica Acta*, **47**: 1247-1275.

Brown P.E. 1989. Flincor: a microcomputer program for the reduction and investigation of fluid inclusion data. *American Mineralogist*, **74**:1390–1393.

Burke E.A.J. 1991. Raman microspectrometry of fluid inclusions: the daily practice. *In*: DeVivo B. & Frezzotti M.L. (eds) *Fluid Inclusions in minerals: methods and applications*. Short Course volume. Virginia Tech, Blacksburg, 25-44 p.

Carvalho J.M.A., Faraco M.T.L., Angélica R.S., Costa M.L. 1991. Problemas em prospecção geoquímica na Região Amazônica: o Projeto RENCA. *In*. SBG, Simpósio de Geologia da Amazônia, 3, *Anais,* p. 395-410.

Chacko T., Hu X., Mayeda T.K., Clayton R.N., Goldsmith J.R. 1996. Oxygen isotope fractionations in muscovite, phlogopite, and rutile. *Geochimica et Cosmochimica Acta*, **60**: 2595-2608.

Clayton R.N. & Mayeda T.K. 1963. The use of bromine pentafluoride in the extraction of oxygen from oxides and silicates from isotopic analyses. *Geochimica et Cosmochimica Acta*, **27**: 43–52.

Coleman M.L., Shepherd T.J., Durham J.J., Rouse J.E., Moore G.R. 1982. Reduction of water with zinc for hydrogen isotope analysis. *Anal. Chem*., **54**: 993-995.

Collins P.L.F. 1979. Gas hydrates in CO_2-bearing fluid inclusions and the use of freezing data for estimation of salinity. *Economic Geology*, **74**: 1435-1444.

Drummond S.E. & Ohmoto H. 1985. Chemical evolution and mineral deposition in boiling hydrothermal systems. *Economic Geology*, **80**: 126-147.

Faraco M.T.L., Fuzikawa K., Ramboz C., McReath I. 2006. A fluid inclusion study in the hydrothermal volcanogenic sulfide and orogenic gold mineralization at the Serra do Ipitinga, Amazon, Brazil. *Revista Brasileira de Geociências*, **36** (1 – suplemento): 51-58.

Goldfarb R.J., Baker T., Dubé B., Groves D.I., Hart C.J.R., Gosselin P. 2005. Distribution, character, and genesis of gold deposits in metamorphic terranes. *Economic Geology 100th Anniversary Volume*, p. 407-450.

Groves D.I., Goldfarb R.J., Robert F., Hart C.J.R. 2003. Gold deposits in metamorphic belts: overview of current understanding, outstanding problems, future research, and exploration significance. *Economic Geology*, **98**: 1-29.

Hall D.L., Sterner S.M., Bodnar R.J. 1988. Freezing point depressions on NaCl-KCl-H_2O solutions. *Economic Geology*, **83**: 197-202.

Harris C., Stuart Smith H., le Roex A.P., 2000. Oxygen isotope composition of phenocrysts from Tristan da Cunha and Gough island lavas: variation with fractional crystallization and evidence for assimilation. *Contributions to Mineralogy and Petrology*, **138**: 164-175.

Kerrick D.M. & Caldera K. 1998. Metamorphic CO2 degassing from orogenic belts. *Chemical Geology*, **145**: 213-232.

Klein E.L. & Fuzikawa K. (in review). Origin of the CO_2-rich fluid inclusions in the Paleoproterozoic Carará vein-quartz gold deposit, Ipitinga Auriferous District, SE-Guiana Shield, Brazil, and their role in gold mineralization.

Klein E.L., Fuzikawa K., Koppe J.C. 2000. Fluid inclusion studies on Caxias and Areal gold mineralizations, São Luís Craton, northern Brazil. *Journal of Geochemical Exploration*, **71**: 51-72.

Klein E.L. & Rosa-Costa L.T. 2003. Geology of quartz-vein gold deposits in the Ipitinga Auriferous District, northern Brazil, southeastern Guiana Shield. *Géologie de la France*, **2,3,4**: 231-242.

Kotzer T.G., Kyser T.K., King R.W., Kerrich R. 1993. An empirical oxygen- and hydrogen-isotope geothermometer for quartz-tourmaline and tourmaline-water. *Geochimica et Cosmochimica Acta*, **57**: 3421-3426.

Loucks R.R. 2000. Precise geothermometry on fluid inclusion populations that trapped mixtures of immiscible fluids. *American Journal of Sciences*, **300**: 23–59

Lowenstern J.B. 2001. Carbon dioxide in magmas and implications for hydrothermal systems. *Mineralium Deposita*, **36**: 490-502.

Ludwig K.R. 2003. User's manual for Isoplot/Ex version 3.00 – A geochronology toolkit for Microsoft Excel. *Berkeley Geochronological Center Special Publication*, **4**: 70 p.

McCuaig T.C. & Kerrich R. 1998. P-T-t-deformation-fluid characteristics of lode gold deposits: evidence from alteration systematics. *Ore Geology Review*, **12**: 381–453

McReath I. & Faraco M.T.L. 2006. Paleoproterozoic greenstone-granite belts in Northern Brazil and the former Guyana Shield – West African Craton Province. *Geol. USP Série Científica*, **5**: 49-63.

Phillips G.N. & Powell R. 1993. Link between gold provinces. *Economic Geology*, **88**: 1084-1098.

Quigley M., Liangjun Y., Xiaohan L., Wilson C.J.L., Sandiford M., Phillips D. 2006. $^{40}Ar/^{39}Ar$ thermochronology of the Kampa Dome, southern Tibet: Implications for tectonic evolution of the North Himalayan gneiss domes. *Tectonophysics*, **421**: 269-297.

Renne P.R., Swisher C.C., Deino A.L., Karner D.B., Owens T.L., DePaolo D.J. 1998. Intercalibration of standards, absolute ages and uncertainties in $^{40}Ar/^{39}Ar$ dating. *Chemical Geology*, **145**: 117-152.

Rodrigues E.M.S. 1992. Implantação do Método Pb-Pb em Rochas Totais. Exemplos de Aplicação em Rochas da Província Mineral de Carajás. Dissertação de Mestrado em Geologia e Geoquímica, Instituto de Geociências, Universidade Federal do Pará. 128p.

Roedder E. 1992. Fluid inclusion evidence for immiscibility in magmatic differentiation. *Geochimica et Cosmochimica Acta*, **56**: 5-20.

Rosa-Costa L.T., Ricci P.S.F., Lafon J.M., Vasquez M.L., Carvalho J.M.A., Klein E.L., Macambira E.M.B. 2003. Geology and geochronology of Archean and Paleoproterozoic domains of the southeastern Amapá and northwestern Pará, Brazil – southeastern Guyana shield. *Géologie de la France*, **2,3,4**: 101-120.

Rosa-Costa L.T., Lafon J.M., Delor C. 2006. Zircon geochronology and Sm-Nd isotopic study: further constraints for the Archean and Paleoproterozoic geodynamical evolution of the southeastern Guiana Shield, north of Amazonian Craton, Brazil. *Gondwana Research*, **10**: 277-300.

Rosa-Costa, L.T., Lafon, J.M., Cocherie, A., Delor, C. (in pressA). 2008. Electron microprobe U-Th-Pb monazite dating of the Transamazonian high-grade metamorphic overprint on Archean rocks from Amapá Block, southeastern Guiana Shield, northern Brazil. *Journal of South American Earth Sciences*, **26**: 445-462.

Rosa-Costa L.T., Monié P., Lafon J.M., Arnaud N.O. (in pressB). 2009. ^{40}Ar-^{39}Ar geochronology across Archean and Paleoproterozoic terranes from southeastern Guiana Shield (north of Amazonian Craton, Brazil): evidence for contrasting cooling histories. *Journal of South American Earth Sciences*. **27**: 113-128.

Sheppard S.M.F., 1986. Characterization and isotopic variations in natural waters, *in* Valley, J.W., Taylor, H.P., and O'Neil, J.R., eds., *Stable isotopes in High Temperature Geological Processes*, Mineralogical Society of America, Reviews in Mineralogy, **16**: 165-183.

Stacey J.S. & Kramers J.D. 1975. Approximation of terrestrial lead isotope evolution by a two-stage model. *Earth Planetary Science Letters*, **26**: 207-221.

Touret J.L.R. 1991. Fluid inclusions in sedimentary and diagenetic environments. *In*: DeVivo, B. & Frezzotti, M.L. (eds) *Fluid Inclusions in minerals: methods and applications*. Short Course volume. Virginia Tech, Blacksburg, p. 251-269.

Vasquez M.L. & Lafon J.M. 2001. Magmatismo tipo A de 1,75Ga na porção oriental do Escudo das Guianas – estados do Amapá e Pará, Brasil. *In*: SBG. Simpósio de Geologia da Amazônia. 7, CD-ROM.

Vasconcelos P.M., Onoe A.T., Kawashita K., Soares A.J., Teixeira W. 2002. $^{40}Ar/^{39}Ar$ geochronology at the Instituto de Geociências, USP: instrumentation analytical procedures and calibration. *Anais da Academia Brasileira de Ciências*, **74**: 297-342.

Vennemann, T.W. & O'Neil, J.R., 1993. A simple and inexpensive method for hydrogen isotope and water analyses of minerals and rocks based on zinc reagent: *Chemical Geology, Isotope Geoscience Section*, **103**: 227-234.

Yardley B.W.D. & Graham J.T. 2002. The origins of salinity in metamorphic fluids. *Geofluids*, 2: 249-256.

Zartman R.E. & Doe B.R. 1981. Plumbotectonics - the model. *Tectonophysics*, **75**: 135-162.